Multibody Syst Dyn (2018) 42:19–45
DOI 10.1007/s11044-017-9576-5

Design and validation of a multi-body model of a front suspension bicycle and a passive rider for braking dynamics investigations

Oliver Maier[1] · Benedikt Györfi[1] · Jürgen Wrede[2] · Roland Kasper[3]

Received: 17 March 2016 / Accepted: 27 April 2017 / Published online: 1 June 2017

Abstract The global spread of Electric Bicycles (EBs) is increasing more and more. In addition to supporting the ease of cycling, the electric energy available can also be used for innovative braking control systems. The project BikeSafe picks up on this idea and aims at developing an active Braking Dynamics Assistance system (BDA) for EBs equipped with hydraulic brakes. A simulation model taking into account all substantial braking dynamics influences is necessary for the model-based design of the BDA. This paper presents a Multi-Body Model (MBM) of a front suspension bicycle and a passive rider. This MBM has been experimentally validated for in-plane braking dynamics using road tests. It has real-time ability and can therefore be used as a virtual representation of the plant for the model-based design process of the BDA.

Keywords Sustainable mobility · Electric bicycle · Safety system · Braking dynamics · Multibody simulation · Passive rider · Experimental validation · Real-time model

Sponsored by the German Ministry of Education and Research (BMBF)

✉ O. Maier
oliver.maier@hs-pforzheim.de

B. Györfi
gyoben@hs-pforzheim.de

J. Wrede
juergen.wrede@hs-pforzheim.de

R. Kasper
roland.kasper@ovgu.de

1 Institute for Applied Research, Pforzheim University, 75175 Pforzheim, Germany

2 Department of Mechanical Engineering, Pforzheim University, 75175 Pforzheim, Germany

3 Institute of Mobile Systems within the Mechanical Engineering Department, Otto-von-Guericke-University Magdeburg, 39106 Magdeburg, Germany

1 Introduction

ELECTRIC BICYCLES (EBs) have become more and more popular as the electric auxiliary drive facilitates movement in daily life. In addition to assisting the rider during acceleration, the electrical energy can also be used for braking control systems to improve bicycle safety. This is the idea behind the research project BikeSafe. It aims to develop an innovative Braking Dynamics Assistance system (BDA) for EBs equipped with hydraulic brakes. The BDA will target two major accident situations: front wheel lockup and nose-over (falling over the handlebars).

An in-depth analysis on bicycle and rider dynamics is crucial for the development of the BDA. A trekking bike (highest sales volume in Germany [1]) with an electrical auxiliary drive has been built up as a test bike (TB) for this purpose. The TB is equipped with an extensive measuring system to capture the vehicle dynamics behavior during braking. The measuring system consists of several sensors and a data acquisition system. A comprehensive description of the TB can be found in [2]. In addition to road tests, simulation models (SM) are used for the following objectives:

1. Investigation of the braking dynamics with regard to both exemplified accident situations
2. Sensitivity studies on the influence of important parameters like bicycle rider size or weight
3. Model-in-the-Loop (MiL) and Hardware-in-the-Loop (HiL) applications for testing the BDA in early development stages (cf. [3])
4. Reducing the amount of road tests (especially dangerous tests for human test riders)

Several approaches for the simulation of two-wheelers can be found in scientific literature. Cossalter et al. [4] and Sharp et al. [5–8] perform theoretical examinations on the stability of motorcycles. Studies on the oscillatory behavior of motorcycles are done by Koenen [9]. Ruijs and Pacejka [10] build an SM to analyse the longitudinal dynamics of motorcycles.

To study the self-stabilization of bicycles, Meijaard et al. [11] analyse the linearized equations of motion based on the Whipple model. Kooijman et al. [12] investigate the self-stabilization effects of a bicycle without the gyroscopic and the caster effect. Furthermore Kooijman et al. [13] validate the correctness of several common assumptions with a test bike. Åström et al. [14, 15], Franke et al. [16] and Hand [17] investigate the stability of bicycles in general and Cerone et al. [18] design a control system to stabilize a riderless bicycle.

A comparison of several SMs of bicycles with different suspension concepts is performed by Wu [19]. These SMs also include a complex rider model. Breuer [20] analyses the influence of several design parameters on the vehicle dynamics of a bicycle system including a rider. Waechter et al. [21] investigate the ground induced vibrational stress on a bicycle rider by the use of an SM and experimental data. A mathematical SM of a mountain bike is created by Redfield [22]. He investigates the performance of a mountain bike which is ridden on rough terrain.

Furthermore the interactions of the bicycle and its rider are analysed in scientific literature by Moore's work [23]. His study is related to the riding dynamics and biomechanical aspects of bicycles and the control behavior of the cyclist. Moore et al. [24, 25] also analyses the motion of a cyclist and evaluates the experimental data statistically. Wang and Hull [26] design a model to determine energy losses in the suspension system. In [27] Wang and Hull use vibrational tests to identify stiffness and damping parameters for the arms, legs and the visceral mass of the rider.

In comparison to previous approaches, this paper presents a Multi-Body Model (MBM) of a bicycle with a front suspension and a passive rider. The major focus is on vehicle braking dynamics. The MBM is divided into three main sub models: rider, bicycle with wheels and braking system. All sub models are composed of rigid bodies and frictionless joints, which are intra- and interconnected by kinematic constraints and force elements. Essential modeling characteristics are the in-plane movement of the bicycle (longitudinal and vertical dynamics), the passive motion of the rider during braking situations and the deflection of the fork.

The MBM model presented has been validated by comparing simulation results with road test measurements. In addition, valuable insights into the so far rarely scientifically studied braking dynamics of bicycles can be obtained from the results. Further improvements of the MBM are proposed and an outlook on the next steps of the development is given.

2 Material and methods

2.1 Requirements and software selection

It is imperative to collect both functional and non-functional requirements for a high quality MBM. The most important ones are listed below:

- The virtual MBM and the real TB (plant of the BDA) have to provide the same interfaces for actuators and sensors
- The parameterization of the *rider model* has to be flexible. The use of different datasets of test riders representing the percentile distribution of the population (5th, 50th, and 95th / male and female) shall be possible
- The frame size within the *bicycle model* has to be variable and has to fit to the particular rider size
- The *brake model* within the bicycle model has to provide an interface for importing (validation from experimental data) or implementing (virtual generic manoeuvres) actuation pressure versus time data For validation purposes and model stimulation with generic braking manoeuvres
- Due to the complex interaction between tyre and road surface during emergency braking manoeuvres a commercially available *wheel/tyre model* solution has to be found and reviewed
- The software for modeling the MBM and performing virtual road tests has to be compatible with the existing tool chain. A monolithic approach is recommended, a co-simulation should be avoided.

Therefore MathWorks's Simulink, SimMechanics 2nd Gen, SimHydraulics, SimScape and MF-Tyre from TNO Automotive (Tass International) [28] are used.

2.2 Topology

The purpose of the model is to reproduce the braking behavior of the bicycle. For this task the model has to contain all elements which are relevant for a braking manoeuvre. These are the hydraulic braking system, bicycle, rider and the wheel-ground-contact.

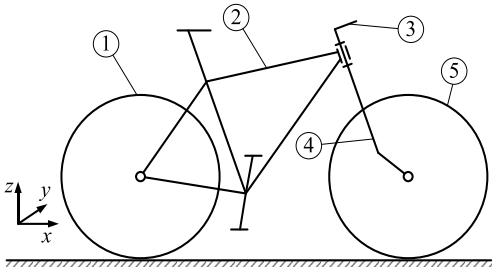

Fig. 1 Mechanical components of a hardtail bicycle

2.2.1 Bicycle and wheels

The brake model for in-depth analysis of bicycle hydraulic disc brakes and its integration into the MBM is described in [29]. Figure 1 shows all five mechanical rigid body components of a front suspension bicycle (called hardtail bicycle): rear wheel (1), frame (2), stanchion tube connected with the handlebar (3), dip tube (4), and front wheel (5).

The handlebar is connected centrically with the stem. The stem itself is connected with the upper end of the stanchion tube. Handlebar, stem and stanchion tube are one rigid body. The connection between stanchion tube and dip tube is a prismatic joint. This joint contains the suspension characteristics of the fork. The connection between fork and frame is done by a locked revolute joint at the stanchion tube (possible model extension concerning lateral dynamics). Both wheels are also connected by revolute joints. The rear wheel connection is located at the rear axle of the frame, the front wheel connection at the lower end of the dip tube. Both wheel models implemented in the MBM use the Pacejka "Magic Formula" tyre model. The road is assumed to have an ideal smooth surface.

2.2.2 Rider

The center of gravity of the rider moves significantly during a braking manoeuvre. This movement has influence on the braking dynamics of the bicycle according to the ratio of rider and vehicle mass. The position of the center of gravity of the rider depends on the limbs and joints of the rider. As a result of this a detailed model of the rider is required. The rider model is based on the following four assumptions: disregarding movement of the collarbone, reduction of the spine to one body, simplifying the skeleton structure to its main functions, and no active muscles. In reality the joints of a human body are very complex [30].

The joints are simplified for modeling purposes as shown in Fig. 2 (cf. [31]). The complex kinematics of the spine are reduced to a revolute joint between the torso (2) and the pelvis (6) with a rotational degree of freedom along the lateral axis. The joint between the torso and the neck (1) is modeled in the same way. In reality shoulder joints include very complex mechanisms. In the model these mechanisms are reduced to the most relevant degrees of freedom represented by a cardan joint. As a consequence, lateral rotation of the upper arms (3) is not taken into account. The hip joint between the torso and the upper legs (7) is modeled in the same way. Knee joints between upper and lower legs (8) and elbow joints between upper and lower arms (4) are represented by revolute joints with rotational degrees of freedom along the lateral axis. Ankles between lower leg and foot (9) and wrists between lower arm and hand (5) are modeled as spherical joints.

During an emergency braking manoeuvre, the deceleration of the bicycle causes a movement of the rider in the direction of travel. An active rider immediately tries to counteract this movement by tensing his muscles. This compensation reaction varies widely between

Fig. 2 Simplified human body

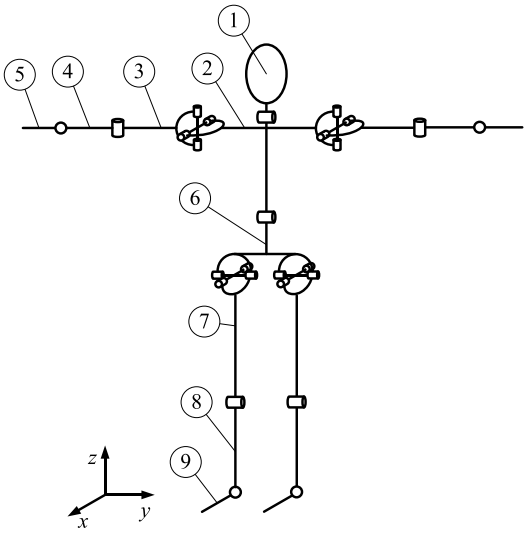

individuals and depends on influences like cycling experience or physical capacity of the cyclist. Due to this variation a generalization is very challenging. In contrast, a passive rider cannot react with a compensation movement. His movement is limited by the basic tension of the musculature. This tension can be parameterized in the MBM using joints with elastic and damping properties. The passive rider model is connected with the bicycle at five spots:

- handlebar-hand-connections with two contact points
- foot-pedal-connections with two contact points
- saddle-pelvic-connection with one contact point

The handlebar-hand connections and the foot-pedal-connections are assumed to be rigid, because there is no relative motion between the elements during normal cycling and braking. For modeling the saddle-pelvic connection two prismatic joints are used. These joints allow both longitudinal and vertical limited translational movements of the virtual rider on the saddle. Figure 3 shows the complete topology of the MBM in a multibody-standardized view. The MBM topology represents a partially closed system with 15 rigid bodies and 19 frictionless joints which results in ten degrees of freedom.

2.3 Modeling

Bicycles are roll-unstable as single-track vehicles and stabilize themselves only due to dynamic effects. As mentioned above, only the in-plane movement of bicycle and rider is modeled within the MBM. For this reason, all components are positioned symmetrically along the longitudinal vehicle middle plane to prevent both from tilting to one side.

2.3.1 Bicycle

To model hardtail bicycles and take their variations into account, an approach is chosen which is comparable to Breuer's approach [20]. The bicycle geometry can be described in relation to the ISO 8855 vehicle coordinate system [32] by defining seven design-independent fixed points (cf. Fig. 4). All fixed points are related to the rear wheel hub. Consequently, the

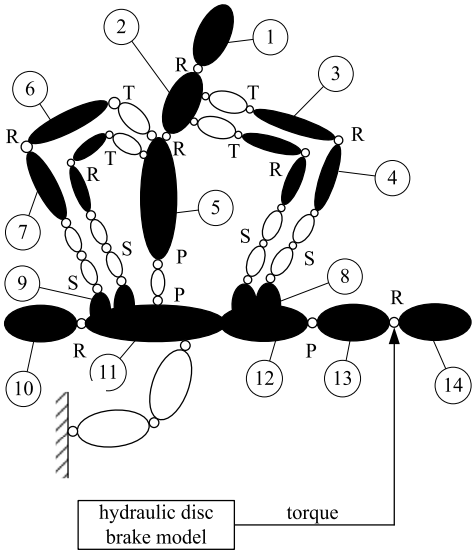

Fig. 3 Topology of the integrated bicycle and rider model

icon	meaning	icon	meaning
1	head & neck	12	stanchion tube & handlebar
2	torso	13	dip tube
3	upper arm	14	front wheel
4	lower arm	⬬	mass body
5	pelvic	⬭	virtual body (massless)
6	upper leg	○	joint (one degree of freedom)
7	lower leg	P	prismatic joint
8	hand	R	revolute joint
9	foot	S	spherical joint
10	rear wheel	T	cardan joint
11	frame		

MBM is able to simulate a wide range of different frame geometries and types of bicycles (e.g. city bikes) just by varying the position parameters of the seven points.

The rear wheel is mounted at the rear axle of the frame at point “A”. Point “B” represents the position of the crankshaft bearing, where both pedals are mounted. The pedals connect the bicycle model with the feet of the rider model. The influence of the pedal position is not taken into account. Both pedals are modeled in a horizontal position.

The steering tube is oriented by the fixed points “C”—intersection with the down tube and “D”—intersection with the top tube. Point “E” is located at the intersection of the top tube and the seat tube. The front wheel is mounted on the lower end of the dip tube at point “F”. Point “G” represents the connection between the saddle of the bicycle model and the pelvis of the rider model.

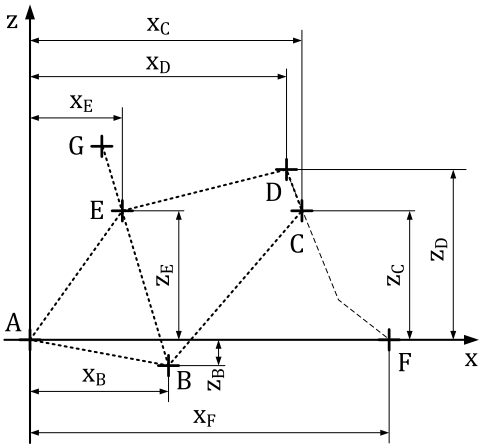

Fig. 4 Geometry points characterizing a hardtail bicycle

2.3.2 *Wheels*

The configuration of the Pacejka tyre model for front and rear wheel (each wheel separated) is performed in the MF-Tyre interface. After opening the respective block, essential settings can be defined: tyre position, calculation method for the tyre-road-interaction, dynamics mode and slip behavior. The wheels of a bicycle are lined up in one plane, so tyre positions are specified symmetrically. A smooth road contact for wheels with a circular cross section (like a motorcycle) was chosen for the tyre-road-interaction. According to several research studies investigating emergency braking manoeuvres [33–35], the dynamics mode was set to non-linear relaxation behavior (relaxation length varies with vertical load and tyre slip) in a frequency range smaller than 10 Hz. Slip behavior was set to combined slip.

2.3.3 *Rider*

The rider model has to be generic and very flexible in its parameterization. In total, seven different riders have to be taken into account. The most important one is the test rider, who carried out all the road tests for validating the MBM. The other six riders represent the percentile distribution of the population (5th, 50th, and 95th / male and female). On the one hand they are needed for sensitivity analyses regarding braking dynamics during both front wheel lockup and nose-over. On the other hand they are used to prove functionality and robustness of the BDA in MiL and HiL applications.

Stiffness and damping properties of the rider are modeled by using linear spring-damper systems. As mentioned in [27], a multi-spring-damper system is mounted on the left and on the right between the wrist and shoulder joints (properties of the elbow) and between the ankle and hip joints (knee). Rotational spring-damper systems are used at the ankle, hip, spine, neck, shoulder, and wrist joints.

2.3.4 *Model fusion and simulation design*

The integrated bicycle and rider model has some essential interfaces (cf. Fig. 5). The most important interfaces are the driving and braking torques. The driving torque accelerates the bicycle and is applied to the rear wheel. In contrast, the braking torque is applied to the front

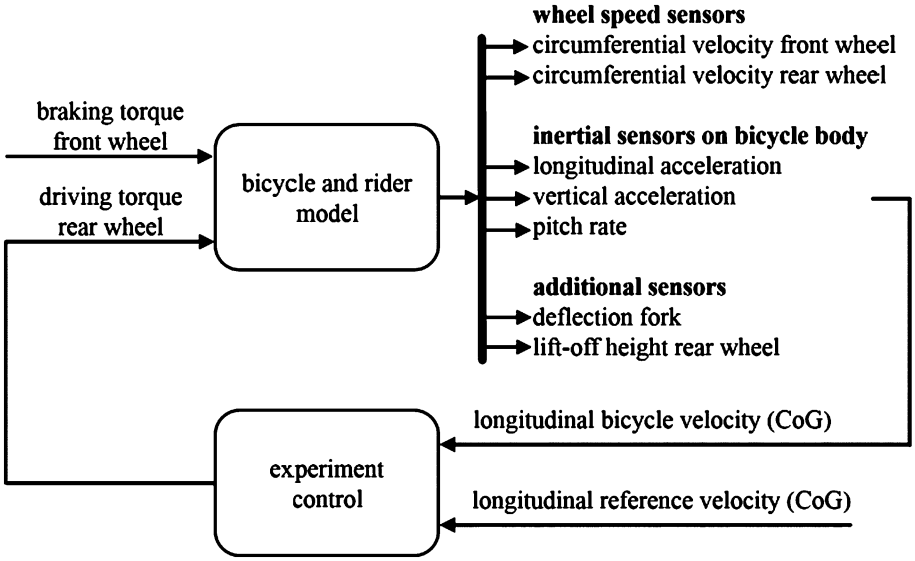

Fig. 5 Virtual test environment with inputs and outputs

wheel and decelerates the bicycle. Thus, the braking torque on the front wheel causes both critical cycling situations: front wheel lockup and nose-over.

A typical simulation run is divided into five sequences:

1. *Starting:* Subsiding of transient oscillations at the beginning of a simulation run.
2. *Accelerating:* A drive torque is applied to the rear axle. The drive torque is set to zero as soon as bicycle and rider reach the initial velocity for braking.
3. *Free-rolling:* Main purpose is to reach an equilibrium condition before the braking manoeuvre starts.
4. *Braking:* Using the actuation pressure versus time data, the brake model calculates a braking torque and applies it to the front axle.
5. *Stopping:* The simulation stops as soon as the actuation pressure time series ends.

According to the equation of linear vehicle motion the sum of all driving resistances equals the sum of traction and brake forces. In comparison to motorized vehicles, the cross-section area of rider and bicycle is smaller and bicycles move significantly more slowly especially when braking to a standstill. For this reason, the influence of air drag (less than 5% share of the total longitudinal deceleration at 30 km/h) is disregarded within the MBM. Rolling resistance forces are calculated using the Pacejka tyre model. By specifying a gradient in the road model—part of Pacejka tyre model—the gravity acceleration vector of the world coordinate system is automatically rotated by SimMechanics. Therefore, the climbing resistance can be calculated easily.

The unknown quantity regarding the equation of linear motion is the vehicle acceleration. In order to solve the equation for braking cases, brake forces have to be calculated on both wheels. The BDA targets only critical driving situations caused by overbraking the front wheel. Consequently, only those brake manoeuvres are taken into account by the MBM. Output of the brake model [29] is a braking torque on the front wheel. This torque is converted into a circumferential brake force by the tyre model.

Table 1 Allocation of riders to frame sizes

No.	Rider		Frame size in cm
1	test rider		61
2	5th	male	50
3	50th	male	56 (54)
4	95th	male	61 (59)
5	5th	female	46 (47)
6	50th	female	51
7	95th	female	56

A particular modeling challenge is a front wheel stop or rotation relative to the other bicycle components. During such a situation the brake disc does not move relative to the brake pads and we get adhesive friction between both friction bodies. As a result, the brake torque is equal to the effective wheel torque, but with inverted algebraic sign. Only if the effective wheel torque becomes larger than the maximum brake torque, the front wheel starts turning forward again. In this (normal) state, the brake torque acts in opposite rotational direction to the wheel due to sliding friction.

A numerical problem with this effect is the discontinuity of the friction force at a change of algebraic sign. If a smooth transition of the friction force is implemented for numerical compatibility, this may lead to reduced friction forces at low wheel speeds, which can influence the results. According to findings in preliminary investigations and [36], Eq. (1) is the best possible solution regarding a continuous description of a friction force F_F. μ represents the coefficient of friction, F_N the normal load, v the current wheel speed, and v_Char the characteristic threshold speed (in this study: $v_\mathrm{Char} = 0.01$ km/h).

$$F_\mathrm{F} = \frac{2}{\pi} \cdot \mu \cdot F_\mathrm{N} \cdot \arctan\left(\frac{v}{v_\mathrm{Char}}\right). \tag{1}$$

2.4 Selection of parameters

2.4.1 Bicycle

Most bicycle parameters depend on frame size. Consequently, the frame size for each of the seven riders has to be determined. According to the common rule in bicycle science "inseam length $\cdot$ 0.66 $\approx$ frame size", all riders can be assigned to a specific frame size [37]. The closest frame sizes to those available on the market (calculated values in brackets) were chosen (cf. Table 1).

The position of the fixed points was derived from data sheets or measured directly in reference to the vehicle coordinate system on all selected bicycles. The distance between the crankshafts bearing (fixed point "B") to the saddle (fixed point "G") is called the saddle height and can be calculated directly by inseam length $\cdot$ 0.9 $\approx$ saddle height [38]. All bicycle components which are independent of the fixed points e.g. geometry of the crank set, were measured at the TB. It is assumed that these independent components are the same for all frame sizes. Both mass and center of gravity locations were measured using the force plate method. Moments of inertia of the bicycle components were measured with an in-house developed test bench using the principle of torsional oscillations [39].

The fork mass, center of gravity location and moment of inertia could not be measured. To determine those parameters a CAD model consisting of dip and stanchion tube

has been built. Stiffness and damping properties of the fork suspension were determined by one of BikeSafe's partner companies, Gustav Magenwirth GmbH & Co KG (better known as Magura). All tests were carried out on a customized test bench in accordance with ISO 4210 [40].

2.4.2 Wheels

Two separate datasets are necessary for the parameterization of the Pacejka tyre model: tyre properties (TIR) and ground definition (RDF). TIR includes geometric and physical wheel and tyre properties as well as the Pacejka coefficients for the tyre-road-interaction.

No longitudinal adhesion-slip curves have been published in the scientific literature for bicycles. Most previous research like the work of Doria [41, 42] or Dressel [43–45] deals with lateral dynamics. For this reason, the longitudinal adhesion-slip curves (depending on wheel speed, wheel load, inflation pressure, and dry and wet road conditions) for TB's Schwalbe Marathon Supreme were measured at an internal drum test bench [46]. In order to avoid too big wheel load variations, a road surface with small height differences called Safety-Walk was used.

The results show similar longitudinal and vertical characteristics as known from motorized vehicles. Due to significant differences of Safety-Walks' macro and micro roughness, the measured adhesion-slip curves were not used for the curve fitting process to determine the Pacejka coefficients. For this reason, the motorcycle tyre dataset 120/70 ZR17 provided with the Pacejka tyre model was modified for a bicycle tyre.

Initially, the adhesion friction coefficient $\mu_{x,\mathrm{A}}$, the corresponding critical slip $\lambda_{\mathrm{B,c}}$, and the sliding friction coefficient $\mu_{x,\mathrm{S}}$ were estimated from road tests for different road surfaces. These gave the following variety of tyre-road-interactions: good, normal, bad, and worst grip. Using Burckhardt's formula for generating generic adhesion-slip curves [47], the Pacejka coefficients within the motorcycle tyre dataset were adapted and evaluated for typical bicycle stationary and transient wheel loads (cf. Fig. 6).

As mentioned above, TIR also includes geometric and physical parameters like mass, moments of inertia, and both radial stiffness and damping coefficients. Geometries, moments of inertia, mass and center of gravity positions of both wheels have been measured. A variety of radial stiffness and damping coefficients can be found [19–22] in the literature. For this reason, radial stiffness and damping coefficients for the TBs' tyres were also measured and checked for plausibility with literature data [46].

Data for RDF contain road coordinates. These coordinates describe the ground profile within an x–z-coordinate system (x is equal to the longitudinal axis, z is equal to the vertical axis in the global coordinate system). The main advantage is that any ground profile can be created. An even road without slope is specified for the validation of the model.

2.4.3 Rider

Most of the riders' parameters representing the percentile distribution of the population can be found in the literature published by the National Aeronautics and Space Administration (NASA) in the United States [48]. NASA data contain geometry, center of gravity location, mass and moments of inertia for every limb of the human body. Parameter gaps were tackled using geometry-based scaling of the existing parameters.

A big issue was the parameterization of the test rider model. Primarily, geometric (e.g. body height) and physical proportions (e.g. total mass) of the test rider were measured. It was assumed that the mass distribution of the test rider (corresponds ca. to 75th percentile

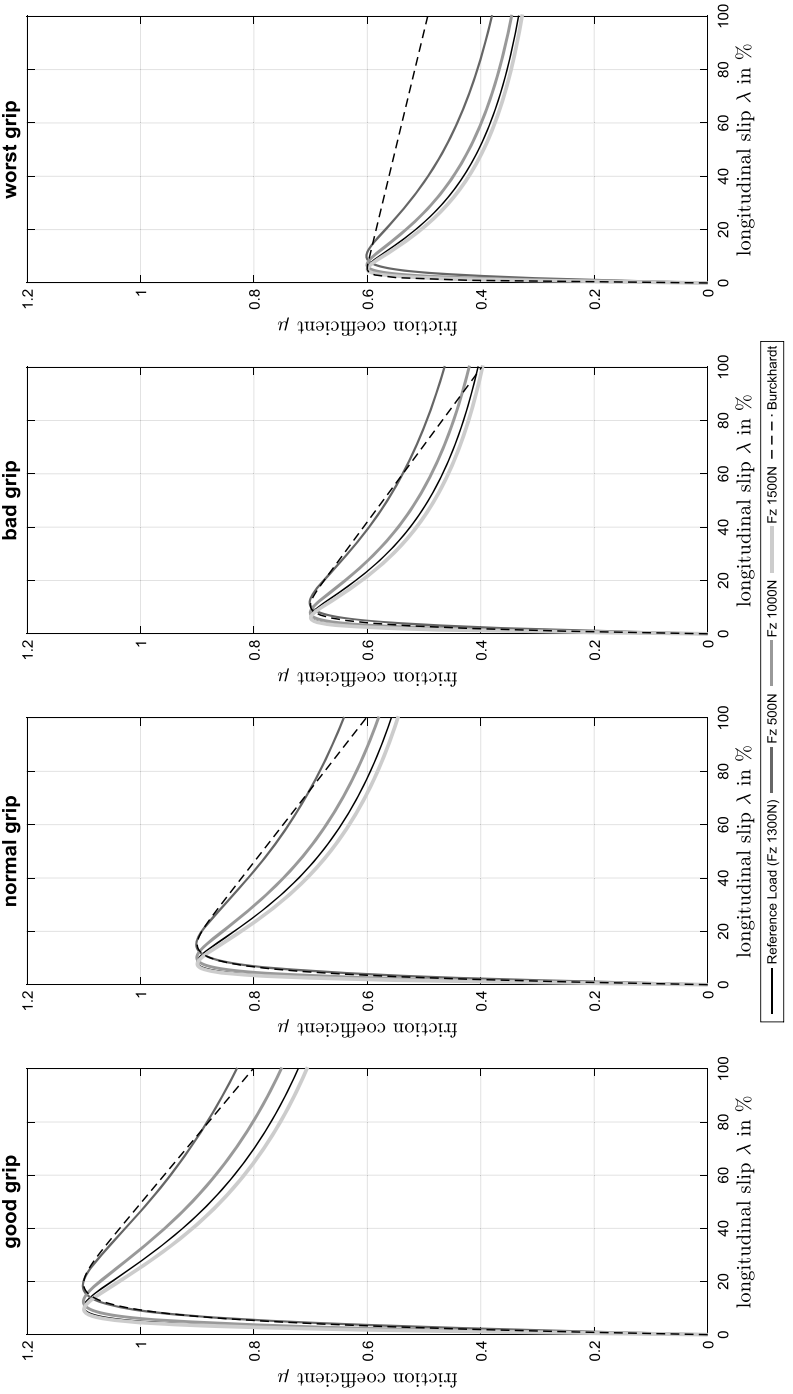

Fig. 6 Adhesion-slip-curves for different road surfaces

male) can be derived from the measured percentile distribution within the NASA dataset. Center of gravity locations and moments of inertia for all limbs were determined by scaling them based on the existing parameters. To validate both mass and center of gravity location of the test rider model, the wheel loads of the TB with the test rider were measured and compared with the wheel loads within the MBM. Validating the moments of inertia has not been possible so far, but resulting errors are assessed as not being relevant due to the plausible range of the calculated values.

Parameters for all linear spring-damper systems originate from the publication [27], parameters of the rotational spring-damper systems from [49]. An accurate scaling of these parameters is not possible. Consequently, all rider models have the same stiffness and damping properties.

3 Validation of the model

The BDA targets the prevention of two major bicycle accident situations: front wheel lockup and nose-over. For this reason, both braking manoeuvres are taken into account for validation. Furthermore, as a braking manoeuvre with reduced vehicle dynamics, strong braking not leading to a critical situation is addressed. Every braking manoeuvre is validated for different bicycle speeds: 10, 15, 20, and 25 km/h. All parameters of the test bike used for validation are presented in Table 2.

Prior to the validation, measurement data captured by the TBs' sensors and recorded by the data acquisition system were analysed. Video data recorded by a high-speed camera with a comparable rate as the sensor data allowed evaluation of active compensation reactions by the test rider.

3.1 Strong braking

All strong braking manoeuvres without a critical riding situation were performed in a car park on a plain, dry concrete road surface (cf. Fig. 6, normal grip). Deflection of the front wheel suspension was allowed (lock-out not activated), only the front wheel was braked with medium brake lever activation by the test rider.

Figure 7 shows the hydraulic actuation and brake pressures, front and rear wheel speeds, pitch rate of the bicycle body, lift-off height of the rear wheel, deflection of the fork, and longitudinal acceleration of the bicycle body, all in a clockwise direction, for a 15 km/h road test and simulation run. All graphs are scaled with respect to typical values as they are measured during both critical braking situations.

As can be seen, there are only small differences between both curves of the front wheel velocity. When the virtual front wheel approaches low travel speed some numerical inaccuracies occur. The discrete real signal is gained by the front wheel speed sensor of the TB evaluated with a fixed-position algorithm and a standstill detection. Unfortunately, only after completion of road tests, it was realized that an event-based sampling of the sensor output within the data acquisition system (hardware-interrupt) would have led to a higher signal quality.

As expected, virtual and real brake pressure courses are identical as the brake pressure signal is the braking manoeuvre stimulation for the MBM.

Comparison of longitudinal acceleration points out remarkable effects. First of all, there are significant oscillations on the real signal. These oscillations are natural oscillations of bicycle and rider with a frequency of approximately 10 Hz. Nevertheless, as the virtual

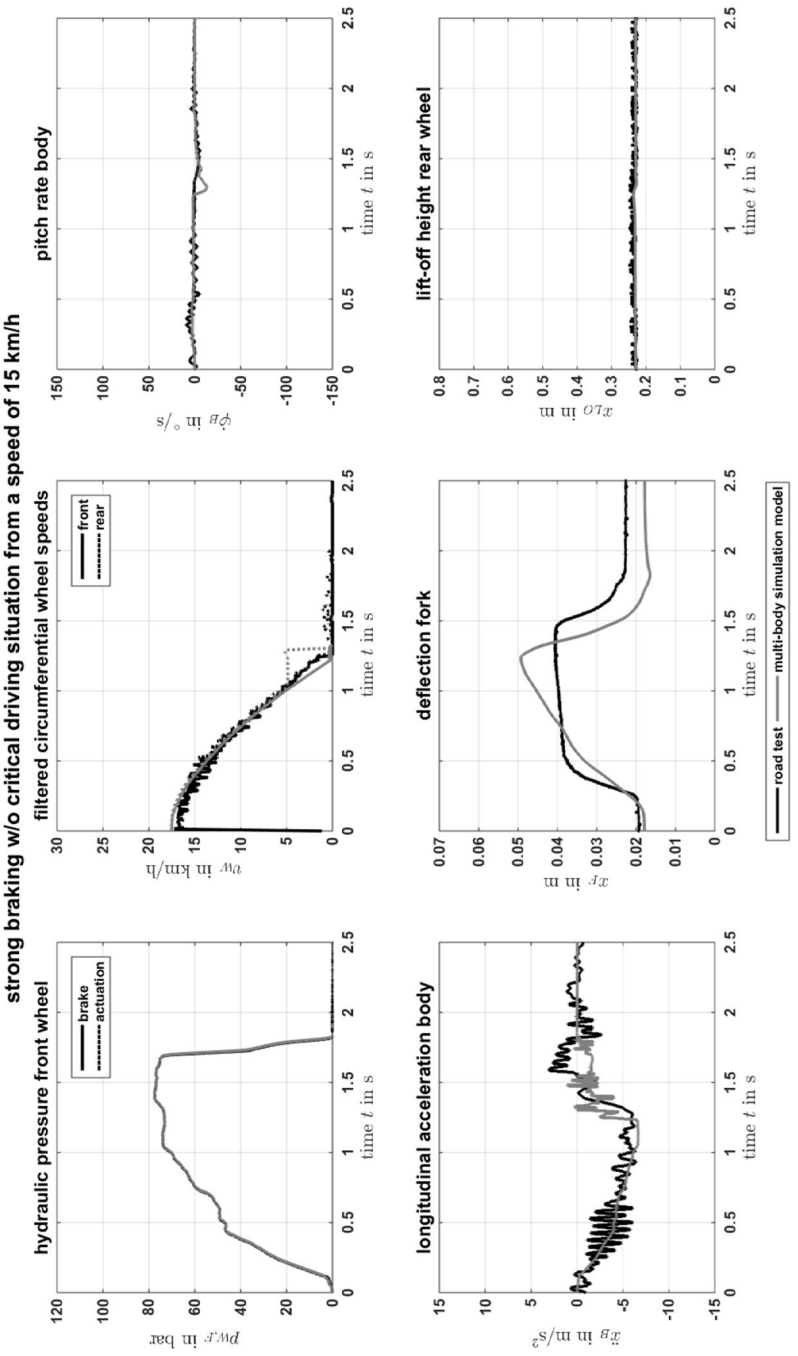

Fig. 7 Strong braking without critical driving situation

longitudinal acceleration is the average of the real oscillating longitudinal acceleration, it can be concluded that the MBM calculates the longitudinal acceleration correctly. Secondly, only the virtual longitudinal acceleration falls below the critical longitudinal deceleration for rear wheel lift-off (approximately $\ddot{x}_C = -6.4\ \mathrm{m/s^2}$ [50]). Although the rear wheel of the MBM lifts off a little bit (step in the rear wheel speed signal), the rear wheel lift-off height is almost constant for both virtual and real courses. Thirdly and lastly, there are some deviations on the longitudinal acceleration courses when the front wheel comes to a standstill. These deviations are caused by the rider removing his feet from the pedals as well as the aforementioned numerical inaccuracies at low travel speed.

As the pitch rate is scaled with respect to a typical nose-over motion only slight deflections can be identified. These deflections are mainly caused by the deflecting fork and can only be seen on flat road surfaces.

The biggest deviations between virtual and real courses can be seen for the fork deflection. On the one hand the graph of the real fork deflection shows clear plateaus, whereas the virtual fork deflection shows the typical linear mass-spring-damper system behavior. The plateaus indicate a distinctive stick-slip effect of the suspension. As a consequence, there are some remarkable differences in the negative suspension travels (called sag) as well.

3.2 Nose-over motion

All braking manoeuvres with a subsequent rear wheel lift-off were performed on a professional test track with a plain, dry, and asphalted road surface (cf. Fig. 6, good grip). Except for an initial velocity prior to braking of 20 km/h all test run boundary conditions were the same as in the case of strong braking. Consequently, Fig. 8 shows the same signals as Fig. 7 in a clockwise direction.

Comparing virtual and real curves of front wheel velocity and longitudinal acceleration, deviations can be recognized. Particularly noteworthy is the jagged graph of the real longitudinal acceleration. Despite the modeling of TBs' sensors internal signal processing, virtual and real signal quality are substantially different. There are manifold reasons for these differences. Primarily, the MBM is composed of rigid bodies, whereas the real bicycle (frame's and fork's elasticity) and rider (flabby mass) are deformable. Secondly, external interference factors from the environment e.g. road surface excitations are disregarded in the MBM as the road is assumed to have an ideal smooth surface. In summary, virtual and real courses of the longitudinal acceleration are on average close to each other. The significant rashes in both courses at the end of the brake manoeuvre are caused by the landing of the rear wheel. Since virtual and real rear wheels lift off and land concurrently, both time periods of nose-over motion are equal.

Furthermore, virtual and real pitch rates as well as rear wheel lift-off heights match quite well. Thus characteristic movement patterns of bicycle and rider during nose-over motion are modeled with good accuracy. Due to the high dynamics of nose-over motion and the associated high forces acting on bicycle and rider, the stick-slip effect of the suspension only slightly influences real fork deflection. Consequently the lack of stick-slip effect of the suspension within the MBM does not distort the outcomes regarding nose-over motion.

3.3 Front wheel lockup

All braking manoeuvres with front wheel lockup were performed on a professional test track with a plain, wet, and polished concrete road surface (cf. Fig. 6, worst grip). As in the road tests before, fork deflection was permitted and only the front wheel was braked. As opposed

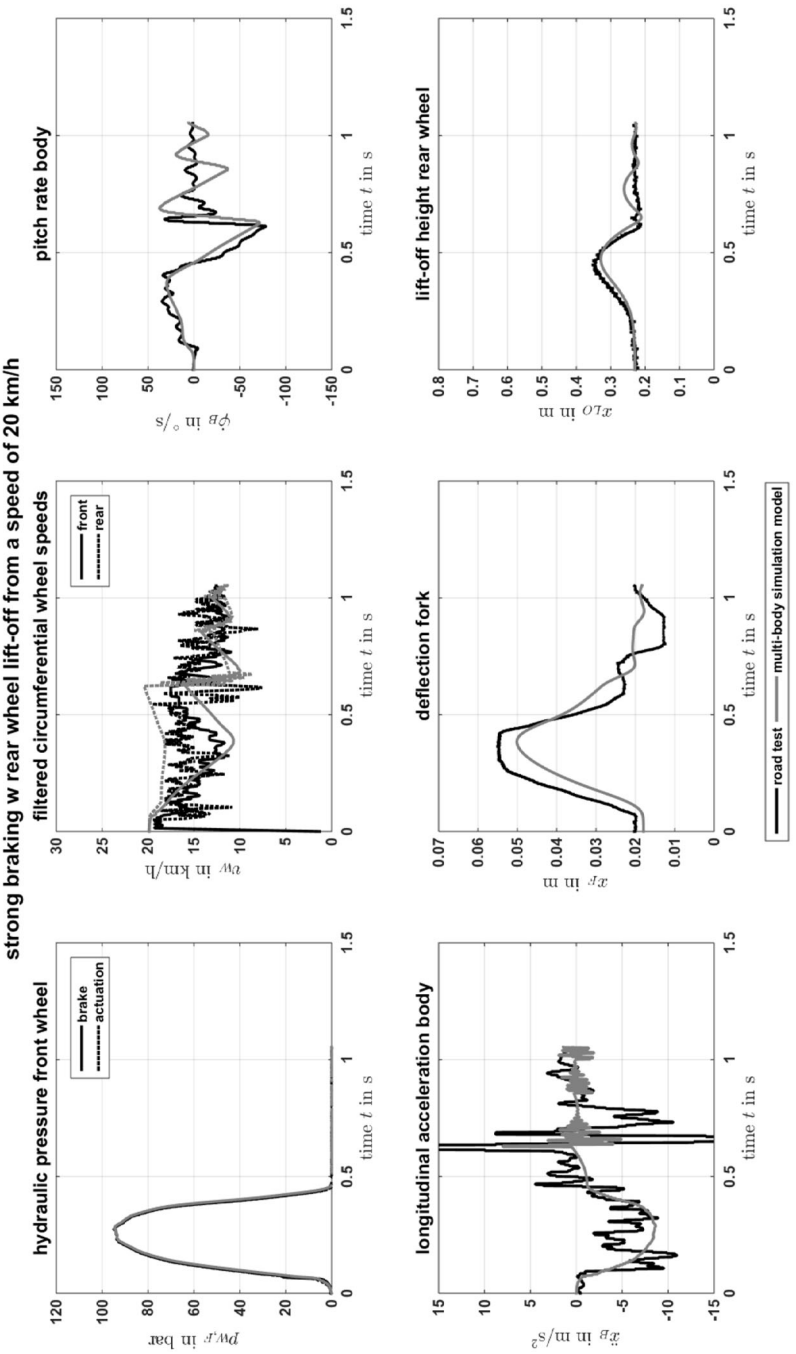

Fig. 8 Strong braking with rear wheel lift-off

to previous road tests brake pressure was specified as high and the TB was equipped with training wheels in order to reduce the risk of falling for the test rider.

Figure 9 shows the hydraulic actuation and brake pressures, front and rear wheel speeds, longitudinal brake slip of the front wheel, lift-off height of the rear wheel, deflection of the fork, and longitudinal acceleration of the bicycle body, all in a clockwise direction, for a 20 km/h road test and simulation run. Besides the MBM, Fig. 9 shows virtual signal courses calculated by a simple Equation-Based Model (EBM) built in MathWorks' Simulink [51].

At the beginning of the braking manoeuvre, both virtual and real front wheel velocities drop. As velocities on the rear wheel, where braking is not applied, decrease only slightly, the calculated virtual and real brake slips on the front wheel increase in the same way. Approximately after 100 ms virtual and real front wheels come to a standstill and begin to slide, because the rear wheel velocities are not equal to zero. During this phase of front wheel sliding, the sliding friction coefficient $\mu_{x,\mathrm{S}}$ defines the tyre-road-interaction.

As the comparison of longitudinal accelerations shows, the MBM reaches the smallest deceleration during front wheel sliding. The EBM, which is parameterized by the adhesion-slip curves calculated with Burckhardt's formula, shows a better match with the real deceleration. This is due to the fact that the sliding friction coefficient $\mu_{x,\mathrm{S}}$ of the adhesion-slip curve by Burckhardt is significantly higher than the adapted curve based on Pacejka coefficients (cf. Fig. 6, worst grip). Consequently, the velocity of the rear wheel within the MBM decreases less than the velocity within the EBM. When the test rider decreases the brake pressure, all front wheels start spinning again. Due to the smaller deceleration of the MBM, the front wheel reaches a higher velocity than the EBM and the real TB.

Comparing virtual and real fork deflections, there are some remarkable differences. As can be seen, due to the small forces acting on the vehicle body during front wheel lockup, the previously identified stick-slip effect of the suspension distorts the outcomes. However, when disregarding the deviations of fork deflection, the main weakness of the MBM for the BDA development is the too small sliding friction coefficient. To solve this restriction, new Pacejka coefficients have to be determined using a curve fitting process for wet polished asphalt.

4 In-depth analysis of road-test data

The results of the previous section show validation of the MBM. In this study, validation is understood as the confirmation by objective evidence that the requirements for a particular application or a particular use are met [52]. Thus, for a meaningful evaluation of the MBM validation, it is necessary to reflect the main characteristics of the MBM:

- Plane movement (longitudinal and vertical dynamics) of bicycle and rider
- Relative motions of the passive rider's limbs to one another as well as to the bicycle
- Front wheel suspension as is typical for hardtail bicycle suspension kinematics

As these characteristics define the MBM boundaries and capabilities, measurement and video data analysis prior to validation were absolutely necessary to select appropriate road tests from all experimental data.

4.1 Strong braking

Figure 10 shows strong braking manoeuvres without a critical riding situation for different bicycle travel speeds: 10, 15, 20, and 25 km/h. Due to the short distance of acceleration

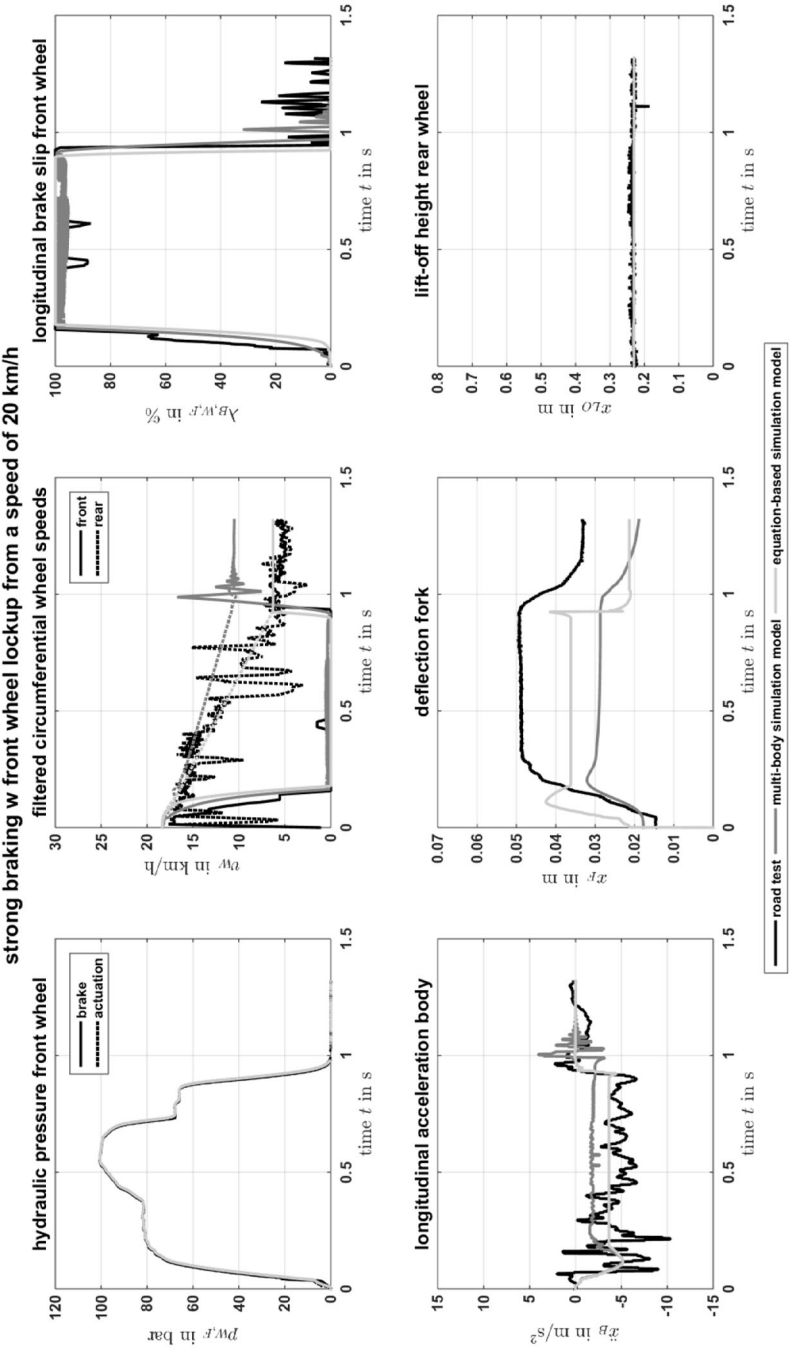

Fig. 9 Strong braking with front wheel lockup

in the car park and the low resolution of the TB's speedometer (one sample per rear wheel revolution), small initial velocities (10 and 15 km/h) prior to braking could not exactly be met by the test rider. This disadvantage suggests that the TB's speedometer display on the handlebars should indicate the wheel speed sensor signal of the rear wheel, which has a much higher resolution (2 times 60 samples per rear wheel revolution).

The specified trapezoidal brake pressure profiles were met satisfactorily. Referring to [39], critical brake pressures for rear wheel lift off with a 75th percentile male (approx. test riders' properties) are in the range of around 80 bars. As Fig. 10 shows, measured brake pressures are close to this limit and rear wheel lift-off height is constant for all test runs. This can only be achieved by professional test riders. However, the test rider could achieve the critical brake pressure that close only for small actuation force and brake pressure gradients, respectively (less than 300 bar/s in regarded test runs).

All graphs are scaled with respect to typical values measured during both critical driving situations. Consequently, it can be stated that prior to and during a braking manoeuvre, the longitudinal acceleration shows a bad signal-to-noise ratio. Due to this fact only a poor correlation between the courses of longitudinal acceleration and brake pressure can be obtained in Fig. 10. In contrast to the longitudinal acceleration, for which effective methods of signal processing (e.g. notch filter) are absolutely vital, the pitch rate's signal-to-noise ratio is sufficient for the BDA function development.

As identified in the validation of the MBM, the TB's fork deflection shows clear plateaus and thus indicates a distinctive stick-slip effect of the suspension. The fork deflection curves in Fig. 10 prove this hypothesis. As can be seen, negative suspension travels (sags) of each road test prior to and at the end of a braking manoeuvre show remarkable differences. Furthermore, there is only a poor correlation between the courses of fork deflection and brake pressure. Due to the unchanged vehicle properties during road tests, bicycle and rider should have the same state of equilibrium prior to and at the end of a braking manoeuvre.

4.2 Nose-over motion

In braking manoeuvres with subsequent nose-over motion, initial velocities prior to braking were met more exactly by the test rider (cf. Fig. 11). This was possible due to a long acceleration distance on the professional test track. Regarding the courses of brake pressure, it is striking that the test rider modulates brake pressures significantly during 10 and 15 km/h road tests. Taking the rear wheel lift-off heights into account, it can be stated that the test rider modulates brake pressure depending on nose-over risk. Logically, the larger the lift-off height, the longer the braking manoeuvre time. During the rear wheel lift-off braking manoeuvres, brake pressure gradients were larger than 700 bar/s. These high gradients were intended to reproduce typical emergency and panic braking manoeuvres during the road test design, at which nose-over accidents mainly occur [53].

At the moment of rear wheel landing there are significant peaks in the courses of longitudinal acceleration as well as pitch rate. These peaks enable easy comparison of both signals with the rear wheel lift-off height. As expected, in all road tests the pitch rate's zero crossing corresponds to the maximum of lift-off height. The significant jumps within the lift-off height are caused by signal dropouts. These dropouts arise when the laser triangulation measurement is disrupted by road surface asymmetries (laser beam deflection) as well as out-of-range error at very high pitch angles.

Besides measurement data, video data analysis was crucial to select appropriate road tests for MBM validation. Because the rider within the MBM is modeled as passive (reactive behavior on external forces), active compensation reactions by the test rider during road

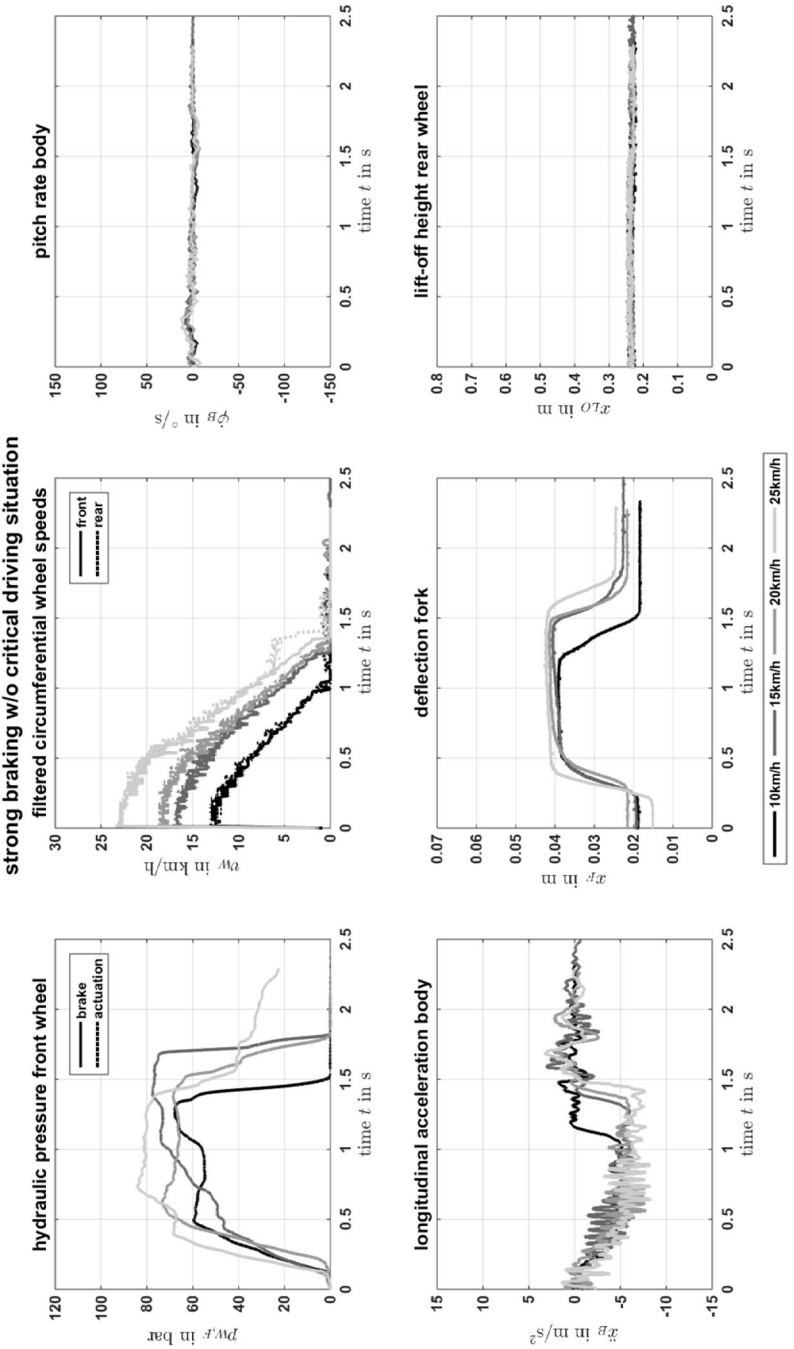

Fig. 10 Strong braking without critical driving situation

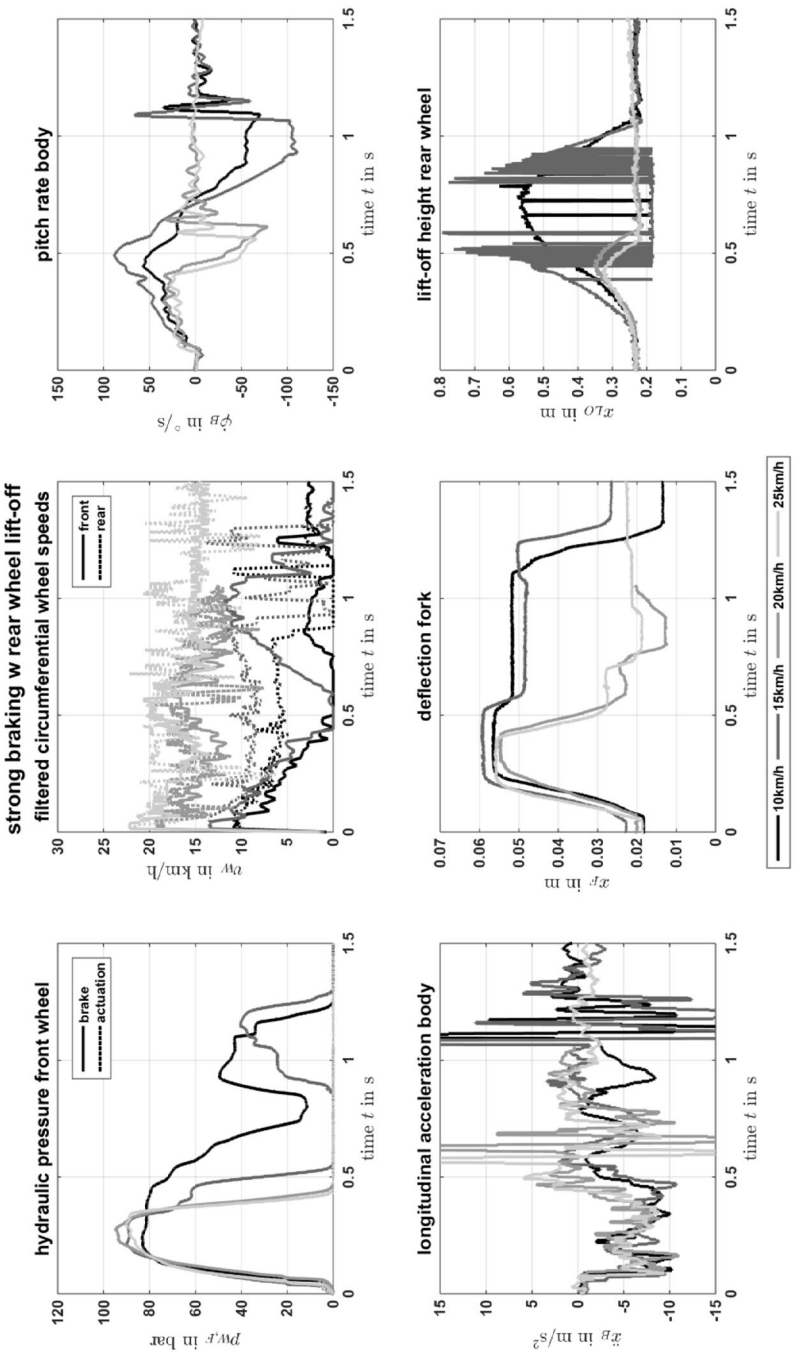

Fig. 11 Strong braking with rear wheel lift-off

tests distort the validation outcomes. It became apparent that the test rider shifts his center of gravity as well as straightens up his upper body in road tests with high nose-over risk (recognizable by high pitch angles on video data and high lift-off height on measurement data). This active rider behavior initiated by internal forces excludes road tests with a high nose-over risk from validation.

4.3 Front wheel lockup

Critical braking manoeuvres with front wheel lockup were also performed for typical bicycle travel speeds: 10, 15, 20, and 25 km/h (cf. Fig. 12). Due to the high dynamics on the front wheel, every test was repeated three times in order to achieve a higher validity of the road test measurements. It should be noted that the shown test run for MBM validation (cf. Fig. 9) was performed with an initial velocity prior to braking of 20 km/h for the response time definition of the anti-lock braking control within the BDA. Thus, the time span to a standstill of the front wheel at lower travel speed is significantly smaller than the identified 100 ms.

At the beginning of both braking manoeuvres rear wheel velocities are not equal to zero. Furthermore front wheel velocities drop. Consequently, longitudinal brake slips increase to 100% and thus the front wheels lock up. In the worst case, the front wheel comes to a standstill after approx. 70 ms. While the brake slips increase, the rear wheel lift-off heights increase as well. As a consequence, rear wheel lift-off and front wheel lockup happen at the same time and superimpose each other. This superimposition occurs whenever the sliding friction coefficient μ_S causes a higher deceleration $\ddot{x}$ than necessary for nose-over motion $\ddot{x}_{NO}$ [54].

As can be seen in Fig. 9, the rear wheel lift-off height is constant for the complete test run. This means the sliding friction coefficient μ_S did not reach the necessary deceleration for nose-over motion $\ddot{x}_{NO}$. The following hypothesis was derived according to these facts: the higher the longitudinal velocity of the bicycle, the lower the adhesion utilization on wet polished asphalt. [55] shows a significant decrease of the adhesion utilization depending on reference velocity for closed and polished road surfaces (little macro and micro roughness) for motor vehicles. Due to a small refloat effect, a water film arises between tyre and road, which is sufficient to separate both friction partners. In case of bicycle tyres and their small contact patch geometries, the refloat effect is assumed to have a smaller but still sufficient impact. Only road tests with exclusive front wheel lockup were considered for validation purposes of the MBM.

5 Conclusion and outlook

The building up of this fully parameterized and validated multibody model (MBM) of a typical electrically assisted hardtail trekking bike including rider has delivered many detailed and important insights into the dynamics of critical braking situations. Examples include influence factors like the dependence between cycling speed and critical braking situations as well as interference factors like excitations by the road surface. Furthermore, the MBM provides one of the most powerful tools for function development of the braking dynamics assistance system (BDA). It can be used as a plant model in model-in-the-loop as well as hardware-in-the-loop simulations. Only the use of such simulation models allows the efficient study of important parameter influences or the design and test of robust control algorithms on the way to a functional prototype.

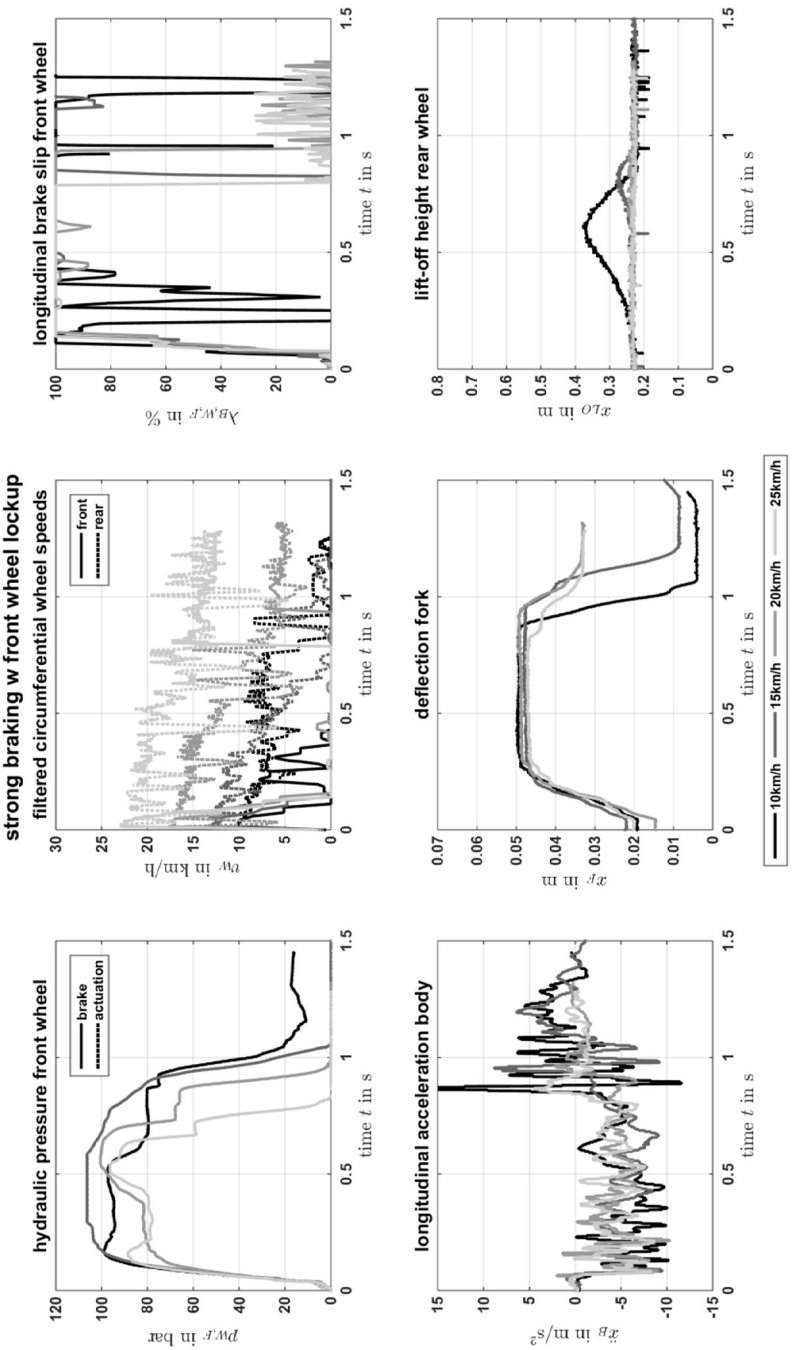

Fig. 12 Strong braking with front wheel lockup

The rider model introduced in this paper is modeled as a passive rider. An active rider model—using muscles for stability and steering purposes—would be an improvement to the existing model. However, this would be a challenging task. The definition of the ground profile can be optimized as well. A smooth surface which is used currently is not a natural situation. Profiles for asphalt, gravel and cobblestones can supplement the results of the MBM and enable more detailed virtual tests of the BDA. Bicycles are typically used for transportation purposes. Consequently, people use luggage racks, backpacks or saddlebags. Defining these extra loads allows investigations regarding the influence of these additional loads on braking behavior. Finally, frame geometries and suspension concepts for bicycles vary greatly. Another further development of the MBM could be the implementation of common suspension concepts like full suspension which is used for many mountain bikes.

Acknowledgements The authors would like to thank the ministry of education and research in Germany (BMBF) for sponsoring the project (FKZ 03FH063PX3). Furthermore, the authors thank all academic and industrial partners for supporting BikeSafe.

Appendix

Table 2 Parameters of the test bike

Quantity	SI-unit	Value
Data acquisition system		
Mass	kg	$m_{\mathrm{DAS}} = 5.7$
Length	m	$l_{\mathrm{DAS}} = 0.29$
Width	m	$w_{\mathrm{DAS}} = 0.34$
Height	m	$h_{\mathrm{DAS}} = 0.15$
Battery pack		
Mass	kg	$m_{\mathrm{BP}} = 2.57$
Inertia (xx, yy, zz)	kg m^2	$I_{\mathrm{BP}} = \begin{pmatrix} 0.004 & & \\ & 0.024 & \\ & & 0.024 \end{pmatrix}$
Center of gravity (x, y, z)	m	$d_{\mathrm{BP,CoG}} = \begin{pmatrix} 0.16 \\ 0 \\ 0.05 \end{pmatrix}$
Length	m	$l_{\mathrm{BP}} = 0.33$
Width	m	$w_{\mathrm{BP}} = 0.09$
Height	m	$h_{\mathrm{BP}} = 0.09$
Distance to drive unit	m	$d_{\mathrm{BP,DU}} = 0.1$
Distance to under tube	m	$d_{\mathrm{BP,UT}} = 0.04$
Frame		
Mass	kg	$m_{\mathrm{F}} = 15.36$
Inertia (xx, yy, zz)	kg m^2	$I_{\mathrm{F}} = \begin{pmatrix} 0 & & \\ & 2.14 & \\ & & 0 \end{pmatrix}$

Table 2 (*Continued*)

Quantity	SI-unit	Value
Center of gravity (x, y, z)	m	$d_{\mathrm{F,CoG}} = \begin{pmatrix} 0.55 \\ 0 \\ 0.18 \end{pmatrix}$
Point A (x, y, z)	m	$d_{\mathrm{F,A}} = \begin{pmatrix} 0 \\ 0 \\ 0 \end{pmatrix}$
Point B (x, y, z)	m	$d_{\mathrm{F,B}} = \begin{pmatrix} 0.46 \\ 0 \\ -0.07 \end{pmatrix}$
Point C (x, y, z)	m	$d_{\mathrm{F,C}} = \begin{pmatrix} 0.93 \\ 0 \\ 0.43 \end{pmatrix}$
Point D (x, y, z)	m	$d_{\mathrm{F,D}} = \begin{pmatrix} 0.87 \\ 0 \\ 0.62 \end{pmatrix}$
Point E (x, y, z)	m	$d_{\mathrm{F,E}} = \begin{pmatrix} 0.28 \\ 0 \\ 0.51 \end{pmatrix}$
Point F (x, y, z)	m	$d_{\mathrm{F,F}} = \begin{pmatrix} 1.10 \\ 0 \\ 0 \end{pmatrix}$
Point G (x, y, z)	m	$d_{\mathrm{F,G}} = \begin{pmatrix} 0.23 \\ 0 \\ 0.67 \end{pmatrix}$
Angle Saddle tube	degree	$\alpha_{\mathrm{ST}} = 73°$
Length Saddle tube	m	$l_{\mathrm{F,S}} = 0.77$
Width Crankshaft	m	$w_{\mathrm{F,C}} = 0.15$
Length Crankshaft	m	$l_{\mathrm{F,C}} = 0.18$
Distance Pedal	m	$l_{\mathrm{F,P}} = 0.3$
Saddle		
Mass	kg	$m_{\mathrm{DAS}} = 5.66$
Inertia (xx, yy, zz)	kg m^2	$I_{\mathrm{BP}} = \begin{pmatrix} 0 & & \\ & 0 & \\ & & 0 \end{pmatrix}$
Center of gravity (x, y, z)	m	$d_{\mathrm{S,CoG}} = \begin{pmatrix} 0 \\ 0 \\ 0 \end{pmatrix}$
Fork		
Mass (handlebar)	kg	$m_{\mathrm{ST}} = 0.33$
Mass (stanchion tube + forkhead + steer tube)	kg	$m_{\mathrm{ST}} = 1.38$
Inertia (stanchion tube + forkhead + steer tube) (xx, yy, zz)	kg m^2	$I_{\mathrm{ST}} = \begin{pmatrix} 0.041 & & \\ & 0.036 & \\ & & 0.005 \end{pmatrix}$

Table 2 (*Continued*)

Quantity	SI-unit	Value
Center of gravity (stanchion tube + forkhead + steer tube) (x, y, z)	m	$d_{\mathrm{BP,CoG}} = \begin{pmatrix} 0.16 \\ 0 \\ 0.05 \end{pmatrix}$
Mass (dip tube)	kg	$m_{\mathrm{DT}} = 1.48$
Inertia (dip tube) (xx, yy, zz)	$\mathrm{kg\,m^2}$	$I_{\mathrm{DT}} = \begin{pmatrix} 0.057 & & \\ & 0.049 & \\ & & 0.008 \end{pmatrix}$
Center of gravity (dip tube) (x, y, z)	m	$d_{\mathrm{DP,CoG}} = \begin{pmatrix} 0 \\ 0 \\ 0.16 \end{pmatrix}$
Length (stanchion tube)	m	$l_{\mathrm{ST}} = 0.3$
Length (dip tube)	m	$l_{\mathrm{DT}} = 0.32$
Length (steer tube)	m	$l_{\mathrm{SteT}} = 0.2$
Length (fork shaft)	m	$l_{\mathrm{FS}} = 0.23$
Length (rack)	m	$l_{\mathrm{R}} = 0.3$
Length (handlebar)	m	$l_{\mathrm{HB}} = 0.64$
Distance (fork head and front axle)	m	$\mathrm{d_{FH}} = 0.46$
Fork bending	m	$\mathrm{d_{FB}} = 0.03$
Angle (rack to fork shaft)	degree	$\alpha_{\mathrm{R}} = 0.13$
Angle (caster)	degree	$\alpha_{\mathrm{C}} = 18°$
Suspension		
Deflection maximum	m	$d_{\mathrm{D,max}} = 0.063$
Stiffness	$\mathrm{kN\,m^{-1}}$	$c = 25$
Damping	$\mathrm{kN\,s\,m^{-1}}$	$d = 4$
Wheels		
Mass (tube + cladding)	kg	$m_{\mathrm{W,TC}} = 0.5$
Mass rim front	kg	$m_{\mathrm{W,Rf}} = 1.16$
Mass rim rear	kg	$m_{\mathrm{W,Rr}} = 3.08$
Inertia front (xx, yy, zz)	$\mathrm{kg\,m^2}$	$I_{\mathrm{W,f}} = \begin{pmatrix} 0.08 & & \\ & 0.16 & \\ & & 0.08 \end{pmatrix}$
Inertia rear (xx, yy, zz)	$\mathrm{kg\,m^2}$	$I_{\mathrm{W,r}} = \begin{pmatrix} 0.08 & & \\ & 0.16 & \\ & & 0.08 \end{pmatrix}$
Radius front (static)	m	$r_{\mathrm{f}} = 0.353$
Radius rear (static)	m	$r_{\mathrm{r}} = 0.353$
Vertical stiffness	$\mathrm{kN\,m^{-1}}$	$c = 200$
Vertical damping	$\mathrm{kN\,s\,m^{-1}}$	$d = 1$

References

1. Eisenberger, D.: Zahlen-Daten-Fakten zum Deutschen E-Bike-Markt. German Bicycle Industry Association (ZIV), Press Release, Berlin (2015)

2. Maier, O., Pfeiffer, M., Wrede, J.: Development of a braking dynamics assistance systems for electric bicycles: design, implementation, and evaluation of road tests. Trans. Mechatron. **21**(3), 1671–1679 (2015). doi:10.1109/TMECH.2015.2505186
3. VDI 2206. Design methodology for mechatronic systems. VDI 2206:2004-06 (2004)
4. Cossalter, V., Lot, R., Massaro, M.: An advanced multibody code for handling and stability analysis of motorcycles. Meccanica **46**(5), 943–958 (2010). doi:10.1007/s11012-010-9351-7
5. Sharp, R.S.: The stability and control of motorcycles. J. Mech. Eng. Sci. **13**(5), 16–329 (1971). doi:10.1243/JMES_JOUR_1971_013_051_02
6. Sharp, R.S.: The dynamics of single track vehicles. Veh. Syst. Dyn. **5**(1–2), 67–77 (1976). doi:10.1080/00423117508968406
7. Sharp, R.S., Limebeer, D.J.N.: A motorcycle model for stability and control analysis. Multibody Syst. Dyn. **6**(2), 123–142 (2001). doi:10.1023/A:1017508214101
8. Sharp, R.S., Evangelou, S., Limebeer, D.J.N.: Advances in the modelling of motorcycle dynamics. Multibody Syst. Dyn. **12**(3), 251–283 (2004). doi:10.1023/B:MUBO.0000049195.60868.a2
9. Koenen, C.: The dynamic behaviour of a motorcycle when running straight ahead and when cornering. Ph.D. dissertation, Dept. Mechanical Engineering, Delft University of Technology, Delft, Netherlands (1983)
10. Ruijs, P.A.J., Pacejka, H.B.: Recent research in lateral dynamics of motorcycles. Veh. Syst. Dyn. **15**(1), 467–480 (1986). doi:10.1080/00423118608969155
11. Meijaard, J.P., Papadopoulos, J.M., Schwab, A.L.: Linearized dynamics equations for the balance and steer of a bicycle: a benchmark and review. Proc. R. Soc. A **436**, 1955–1982 (2007). doi:10.1098/rspa.2007.1857
12. Kooijman, J.D.G., Meijaard, J.P., Papadopoulos, J.M., Ruina, A., Schwab, A.L.: A bicycle can be self-stable without gyroscopic or caster effects. Science **332**(6027), 339–342 (2011). doi:10.1126/science.1201959
13. Kooijman, J.D.G., Schwab, A.L., Meijaard, J.P.: Experimental validation of a model of an uncontrolled bicycle. Multibody Syst. Dyn. **19**(1), 115–132 (2007). doi:10.1007/s11044-007-9050-x
14. Åström, K.J., Lunze, J.: Why are we able to ride a bicycle? Automatisierungstechnik **49**(10), 427–435 (2009). doi:10.1524/auto.2001.49.10.427
15. Åström, K.J., Klein, R.E., Lennartsson, A.: Bicycle dynamics and control. IEEE Control Syst. **25**(4), 26–47 (2005). doi:10.1109/MCS.2005.1499389
16. Franke, G., Suhr, W., Rieß, F.: An advanced model of bicycle dynamics. Eur. J. Phys. **11**(2), 116–121 (2000). doi:10.1088/0143-0807/11/2/010
17. Hand, R.S.: Comparisons and stability analysis of linearized equations of motion for a basic bicycle model. M.S. thesis, Cornell University, NY (1988)
18. Cerone, V., Andreo, D., Larsson, M., Regruto, D.: Stabilization of a riderless bicycle a linear-parameter-varying approach. IEEE Control Syst. **30**(5), 23–32 (2010). doi:10.1109/MCS.2010.937745
19. Wu, C.-C.: Static and dynamic analyses of mountain bikes and their riders. Ph.D. dissertation, University of Glasgow, Glasgow (2012)
20. Breuer, J.: Untersuchung des Einflusses geometrischer Parameter auf das Fahrverhalten von Einspurfahrzeugen. M.S. thesis, Dept. Mechanical Engineering and Mechatronic, University of Applied Sciences Aachen, Germany (2013)
21. Waechter, M., Riess, F., Zacharias, N.: A multibody model for the simulation of bicycle suspension systems. Veh. Syst. Dyn. **37**(1), 3–28 (2002). doi:10.1076/VESD.37.1.3.3539
22. Redfield, R.: Large motion mountain biking dynamics. Veh. Syst. Dyn. **43**(12), 845–865 (2005). doi:10.1080/00423110412331289844
23. Moore, J.K.: Human control of a bicycle. Ph.D. dissertation, Dept. Mechanical and Aerospace Engineering, University of California, Davis, CA (2012)
24. Moore, J.K., Hubbard, M., Schwab, A.L., Kooijman, J.D.G., Peterson, D.L.: Statistics of bicycle rider motion. Proc. Eng. **2**(2), 2937–2942 (2010). doi:10.1016/j.proeng.2010.04.091
25. Moore, J.K., Kooijman, J.D.G., Schwab, A.L., Hubbard, M.: Rider motion identification during normal bicycling by means of principal component analysis. Multibody Syst. Dyn. **25**, 225–244 (2011). doi:10.1007/s11044-010-9225-8
26. Wang, E.L., Hull, M.L.: A model for determining rider induced energy losses in bicycle suspension systems. Veh. Syst. Dyn. **25**(3), 223–246 (1996). doi:10.1080/00423119608968966
27. Wang, E.L., Hull, M.L.: A dynamic system model of an off-road cyclist. J. Biomech. Eng. **119**(3), 248–253 (1997). doi:10.1115/1.2796088
28. Besselink, I.J.M.: Vehicle dynamics analysis using SimMechanics and TNO Delft-tyre. In: The MathWorks International Automotive Conference, IAC 2006, Stuttgart, Germany (2006)
29. Maier, O., Györfi, B., Wrede, J., Arnold, T., Moia, A.: In-depth analysis on bicycle hydraulic disc brakes. Mech. Syst. Signal Process. **95**, 310–323 (2017). doi:10.1016/j.ymssp.2017.03.044

30. Schiebler, T.H., Korf, H.W.: Anatomie Histologie, Entwicklungsgeschichte, makroskopische und mikroskopische Anatomie, Topographie (2007). ISBN 978-3-7985-1770-7
31. Schramm, D., Hiller, M., Bardini, R.: Vehicle Dynamics: Modeling and Simulation, pp. 43–73. Springer, Berlin (2014). doi:10.1007/978-3-540-36045-2
32. ISO 8855. Road vehicles—vehicle dynamics and road-holding ability. ISO 8855:2011 (2011)
33. Pauwelussen, J.P.: Full vehicle ABS braking using the SWIFT rigid ring tyre model. IFAC Control Eng. Pract., CEP **11**(2), 199–207 (2003)
34. Jansen, S.T.H., Zegelaar, P.W.A., Pacejka, H.B.: The influence of in-plane tyre dynamics on ABS braking of a quarter vehicle model. Veh. Syst. Dyn. **32**(2–3), 249–561 (1999). doi:10.1076/VESD.32.2.249.2086
35. Jaiswal, M., Mavros, G., Rahnejat, H., King, P.D.: Influence of tyre transience on anti-lock braking. Proc. Inst. Mech. Eng., Proc., Part K, J. Multi-Body Dyn. **224**(1), 1–17 (2009)
36. Popov, V.L.: Kontaktmechanik und Reibung, pp. 309–333. Springer, Berlin (2010). ISBN 978-3-642-13302-2
37. Bellersheim, R., et al.: Tabellenbuch Fahrradtechnik, p. 300. Haan-Gruiten, Europa-Lehrmittel (2014). ISBN 978-3808523336
38. Artmann, U., et al.: Fachkunde Fahrradtechnik, p. 384. Haan-Gruiten, Europa-Lehrmittel (2014). ISBN 978-3808522950
39. Maier, O., Györfi, B., Kubatschek, A., Pfeiffer, M., Wrede, J.: Simulationsgestützte Bewertung kritischer Einflussgrößen auf das Vorderradblockieren bei Elektrofahrrädern. In: ASIM/GI-Fachgruppen Workshop, Stralsund, Germany, June 18–19, 2015 pp. 257–268 (2015). ISBN 978-3-9813334-9-7
40. ISO 4210. Safety requirements for bicycles, part 6: frame and fork test methods. ISO 4210-6:2014 (2014)
41. Doria, A., et al.: Identification of the mechanical properties of bicycle tyres for modelling of bicycle dynamics. Veh. Syst. Dyn. **51**(3), 405–420 (2013). doi:10.1080/00423114.2012.754048
42. Bulsink, V., Doria, A., et al.: The effect of tyre and rider properties on the stability of a bicycle. Adv. Mech. Eng. **7**(12), 1–19 (2015). doi:10.1177/1687814015622596
43. Dressel, A.E.: Measuring and modeling the mechanical properties of bicycle tires. Ph.D. dissertation, The University of Wisconsin-Milwaukee, Milwaukee (2013)
44. Dressel, A.E.: Measuring dynamic properties of bicycle tires. In: Symposium on Dynamics and Control of Single Track Vehicles, Proceedings of Bicycle and Motorcycle Dynamics, Delft (2010)
45. Dressel, A.E., Rahman, A.: Measuring sideslip and camber characteristics of bicycle tires. Veh. Syst. Dyn. **50**(8), 1365–1378 (2011). doi:10.1080/00423114.2011.615408
46. Maier, O., Hillenbrand, S., Wrede, J., Freund, A., Gauterin, F.: Vertical and longitudinal characteristics of a bicycle tire. Tire Sci. Technol. (accepted for publication)
47. Burckhardt, M.: Der Reifen als Regelgröße. In: Fahrwerktechnik: Radschlupf-Regelsysteme, pp. 15–62. Vogel, Würzburg (1993)
48. National Aeronautics and Space Administration. International space station flight. Crew Integration Standard, NASA-STD-3000/T (1999)
49. Kłodowski, A., Rantalainen, T., Heinonen, A., Sievänen, H., Mikkola, A.: The use of the flexible multibody approach for lower body skeletal loading analysis. Proc. IUTAM **2**, 93–100 (2011). doi:10.1016/j.piutam.2011.04.010
50. Cossalter, V.: Rectilinear motion of motorcycle. In: Motorcycle Dynamics, 2nd edn., pp. 73–104 (2006). ISBN 978-1-4303-0861-4
51. Maier, O., Pfeiffer, M., Wrede, J.: Bremsdynamisches Assistenzsystem für elektrifizierte Fahrräder: Aufbau und Validierung eines Umgebungsmodells als Grundlage der modellbasierten Entwicklung. In: VDI Tagung Mechatronik, Dortmund, Germany, March 12–13, 2015, pp. 271–276 (2015). ISBN 978-3-00-048814-6
52. ISO 9000. Quality management systems—fundamentals and vocabulary. ISO 9000:2015 (2015)
53. Bauer, K., Schick, S., Wagner, A., Zhou, K., Peldschus, S., Malczyk, A.: Untersuchungen zur Schutzwirkung des Fahrradhelms. Research report No. 32, German Insurance Association, Berlin (2015)
54. Maier, O., Scharpf, S., Pfeiffer, M., Wrede, J.: Conditions of nose-over and front wheel lockup on electric bicycles. In: 17th Int. Conf. on Research and Education in Mechatronics, Compiègne, France, June 15–17 (2016). doi:10.1109/MECATRONICS.2016.7547145
55. Bachmann, B.: Wechselwirkungen im Prozeß der Reibung zwischen Reifen und Fahrbahn, pp. 45–106. VDI Verlag No. 12/360, Düsseldorf (1998)